The Arctic Ozone Hole in March 2020 and Its Seasonal Prediction in CFSv2: A Comparative Study with the 1997 and 2011 Arctic Ozone Holes

Jian Rao[1] and Chaim I Garfinkel[2]

[1]Nanjing University of Information Science and Technology
[2]Hebrew University of Jerusalem

November 22, 2022

Abstract

Using reanalysis data, observations, and seasonal forecasts, the March Arctic ozone hole events in 1997, 2011, and 2020 and their predictability are compared. All of the three ozone hole events were accompanied by an extremely strong and cold polar vortex. The shape and centroid of the ozone holes are mainly controlled by the simultaneous polar vortex. The March 2020 ozone hole was displaced towards Canada and Greenland, the March 2011 ozone low was evenly distributed over the North Pole, while the 1997 ozone hole was displaceds toward Arctic Russia. The predictability of the 2011 ozone hole event is longer (1–2 months) than the other two (~1 month) possibly due to La Niña and Quasi-Biennial westerly winds, favorable for formation of a strong polar vortex. Surprisingly, an empirical model using a substitute index to forecast the Arctic ozone might be as skillful as the general circulation model with a chemistry module.

Hosted file

`rao et al. 2020-ozone hole-si.docx` available at https://authorea.com/users/535463/articles/598768-the-arctic-ozone-hole-in-march-2020-and-its-seasonal-prediction-in-cfsv2-a-comparative-study-with-the-1997-and-2011-arctic-ozone-holes

1 **The Arctic Ozone Hole in March 2020 and Its Seasonal Prediction in CFSv2: A**
2 **Comparative Study with the 1997 and 2011 Arctic Ozone Holes**

3 **Jian Rao[1,2] and Chaim I. Garfinkel[1]**

4 [1]Fredy and Nadine Herrmann Institute of Earth Sciences, The Hebrew University of Jerusalem,
5 Edmond J. Safra Campus, Givat Ram Jerusalem 91904, Israel

6 [2]Key Laboratory of Meteorological Disaster, Ministry of Education (KLME) / Joint
7 International Research Laboratory of Climate and Environment Change (ILCEC) /
8 Collaborative Innovation Center on Forecast and Evaluation of Meteorological Disasters
9 (CIC-FEMD), Nanjing University of Information Science and Technology, Nanjing 210044,
10 China

11

12 Submitted to *Geophysical Research Letters*

13 (May 2020)

14

15 Corresponding author: Dr. Jian Rao, jian.rao@mail.huji.ac.il

16

17 **Key Points:**

18 • The 1997, 2011 and 2020 March ozone holes were accompanied by an extremely
19 strong and cold polar vortex.

20 • The shape and centroid of the Arctic total ozone holes were controlled by the
21 stratospheric polar vortex.

22 • The 2011 March ozone hole is more predictable than the 1997 and 2020 March ozone
23 hole events, possibly due to favorable ENSO and QBO conditions.
24

25 **Abstract**

26   Using reanalysis data, observations, and seasonal forecasts, the March Arctic ozone hole
27 events in 1997, 2011, and 2020 and their predictability are compared. All of the three ozone
28 hole events were accompanied by an extremely strong and cold polar vortex. The shape and
29 centroid of the ozone holes are mainly controlled by the simultaneous polar vortex. The
30 March 2020 ozone hole was displaced towards Canada and Greenland, the March 2011 ozone
31 low was evenly distributed over the North Pole, while the 1997 ozone hole was displaced
32 toward Arctic Russia. The predictability of the 2011 ozone hole event is longer (1–2 months)
33 than the other two (~1 month) possibly due to a moderate La Niña and Quasi-Biennial
34 westerly winds, favorable for the formation of a strong polar vortex. Surprisingly, an
35 empirical model using a substitute index to forecast the Arctic ozone might be as skillful as
36 the general circulation model with a chemistry module.

37 **Key words:** Arctic ozone hole; stratospheric polar vortex; predictability

38

39 **Plain language**

40   Low total column ozone was observed this past March over the Artic (a so-called "ozone
41 hole"), and its meteorological conditions are compared with the other two similar Arctic
42 low-ozone events in 1997 and 2011. All of the three historical ozone hole events occurred
43 within an unusually strong and cold stratospheric polar vortex, and the shape and centroid of
44 the ozone holes were also consistent with the polar vortex. The ozone hole in March 2020
45 was displaced towards the North American sector, the March 2011 ozone hole was centered
46 over the North Pole, while the 1997 ozone hole displaced toward the Eurasian sector. We also
47 find that the predictability of the 2011 ozone hole event is longer (1–2 months) than the 1997
48 and 2020 March event (~1 month), perhaps due to favorable tropical forcings (e.g., La Niña
49 and westerly QBO). The general circulation model with a chemical module shows a
50 comparable predictive skill for the ozone holes to an empirical model using a substitute index
51 to forecast the Arctic ozone.

52

1. Introduction

During the austral spring, a nearly complete depletion of lower-stratospheric ozone results in an ozone hole over the Antarctic nearly every year (Solomon, 1999; Manney et al., 2011; Rieder et al., 2014). In the Northern Hemisphere, on the other hand, chlorine activation and subsequent Arctic ozone depletion only occur when the stratospheric polar vortex persists into spring and lower stratospheric temperatures are unusually cold (Arnone et al., 2012). Arctic ozone loss therefore has large interannual variability due to large planetary wave disturbances and even sudden warmings which ordinarily prevent long-lived cold temperature in the Northern Hemisphere (Manney et al., 2011). Hitherto, only three Northern Hemisphere "ozone hole" events have been observed since 1979 (i.e., March in 1997, 2011, and 2020 in Fig. 1).

The March 1997 ozone hole (Newman et al., 1997; Zhang et al., 2013) and especially the March 2011 ozone hole (Hurwitz et al., 2011; Liu et al., 2011; Sinnhuber et al., 2011; Varotsos et al., 2012; Arnone et al., 2012; Solomon et al., 2014; Chipperfield et al., 2015) have attracted wide attention. For example, Arnone et al. (2012) analyzed the Arctic dynamics, chemistry, and polar stratospheric clouds during the 2010/11 ozone hole using the limb sounding infrared measurements. Two major processes are responsible for the low ozone in early spring over the Arctic: heterogeneous chemical loss (Solomon, 1999; Hommel et al., 2014; Shaw & Perlwitz, 2014) and a quiescent stratosphere in winter (Olascoaga et al., 2012; Strahan et al., 2013). When the stratosphere is quiescent and the stratospheric westerly jet is strong, the poleward mass transport from the ozone-rich tropics to the ozone-poor polar regions is blocked with the anomalously strong jet serving as a barrier for the ozone transport (Strahan et al., 2013). On the other hand, ozone depletion in the Arctic winter is also dependent on the volume of the polar stratosphere below the temperature threshold for polar stratospheric cloud formation (Rex et al., 2006; Harris et al., 2010; Garfinkel et al., 2015). The Arctic stratospheric temperatures in the 2010/11 winter were one of the coldest (Manney et al., 2011; Sinnhuber et al., 2011). The ozone loss over the Arctic in the 2011 spring was quantitatively comparable to that in the Antarctic ozone hole (e.g., Sinnhuber et al., 2011; Varotsos et al., 2012).

Springs with low Arctic (Antarctic) ozone concentration in March (October) are associated with a strong and cold stratospheric polar vortex, which corresponds to the positive polarity of NAM/NAO (SAM) in early boreal (austral) spring (Thompson & Solomon, 2002; Previdi & Polvani, 2014; Solomon et al., 2014). Both modelling and observational evidence show that the extreme low Arctic stratospheric ozone anomalies in spring are usually accompanied with a poleward shift of the tropospheric westerly jet in the North Atlantic sector and a positive NAO-like circulation pattern (Calvo et al., 2015; Ivy et al., 2017), though the surface impacts may be associated more with the strong vortex that allowed for the low ozone in the first place (Harari et al., 2019). In addition, an ozone hole allows for ultraviolet radiation to reach the surface, which endangers the lives of plants, animals, and humans inhabiting the Arctic. Considering the possible impact of the ozone loss on the near-surface weather and ecosystem (Waugh et al., 2009; Neely et al., 2014), a timely

94   prediction of ozone hole events can be used to warn society.

95   This paper focuses on the general meteorological conditions for the three historical
96   "ozone hole" events in the Northern Hemisphere, although the ozone holes over the Arctic
97   are not as deep as in the Antarctic. Seasonal predictions of the three ozone hole events are
98   compared using operational model output by an operational forecast system. We will show
99   that the predictability of the ozone hole is largely dependent on the representation of the polar
100   vortex in the forecast system for the three Arctic cases.

101   The organization of the paper is as follows. Following the introduction, section 2
102   describes the data, model forecasts, and methods. The background circulation conditions for
103   the three Arctic ozone hole events are shown in section 3. The predictions of the Arctic ozone
104   holes using the empirical method and the forecast model are compared in section 4. Finally,
105   conclusions are presented in section 5.

106   **2. CFSv2 seasonal forecasts, data, and methods**

107   *2.1 NCEP Climate Forecast System version 2 (CFSv2) and its seasonal predictions*

108   As a successor to NCEP CFSv1, the NCEP CFSv2 began to operate on 30 March 2011
109   (Saha et al., 2014). The CFSv2 forecast model is a fully coupled model system with an
110   atmospheric spectral model interacting with ocean, land, and sea ice. The forecast system
111   runs at a T126 (~100 km) horizontal resolution for the atmosphere. This model uses a
112   signal-pressure hybrid vertical coordinate with 64 levels. This model was also used to create
113   the NCEP Climate Forecast System Reanalysis (CFSR). The seasonal reforecasts before 2011
114   by CFSv2 were performed every five days. The reforecasts initialized on the specific days
115   have four members using the initial conditions at 0000, 0600, 1200, and 1800 UTC. The
116   real-time seasonal forecasts were initialized four times (0000, 0600, 1200, and 1800 UTC)
117   per day. The seasonal forecast/reforecast products produced 9-month integrations
118   (https://www.ncdc.noaa.gov/data-access/model-data/model-datasets/climate-forecast-system-
119   version2-cfsv2). CFSv2 is also one of models participating in the subseasonal to seasonal
120   (S2S) program initialized in 2013 by WCRP and WWRP. Recent studies have shown that this
121   forecast system is among the best at predicting sudden stratospheric warming (SSW) events
122   in two hemispheres (Domeisen et al., 2020a, 2020b; Rao et al., 2019, 2020a, 2020b). A full
123   ozone photochemistry scheme is not used in many S2S or seasonal forecast models due to its
124   computational expense, but CFSv2 includes a prognostic ozone parameterization scheme
125   (Compo et al., 2016). Specifically, the time tendency of ozone is specified using the partial
126   CHEM2D Ozone Photochemistry Parameterization (CHEM2D-OPP) method (McCormack et
127   al., 2006).

128   Considering that Arctic ozone hole events in March are persistent with little
129   sub-monthly variability, we focus on the seasonal forecast of the three ozone hole events,
130   rather than the day-by-day forecasts in details. The CFSv2 initializations at the very
131   beginning of each winter month are downloaded and assessed in this study (Table S1).
132   Similar to the winds, height, and air temperature, the total column ozone is also a standard

133   output from the forecast system.

134   *2.2 Reanalysis and observations*

135   The ERA5 reanalysis (Hersbach et al., 2020) is used as the baseline for assessment of
136   the CFSv2 forecasts. The daily and monthly data at a $1.5° \times 1.5°$ horizontal resolution is
137   downloaded from the Copernicus Climate Change Service Climate Data Store after
138   registration (https://cds.climate.copernicus.eu). Variables used in this study include the zonal
139   and meridional winds, air temperature, geopotential (divided by the gravitational acceleration
140   to extract the height), and Ertel potential vorticity at 37 pressure levels (1000–1hPa). The total
141   column ozone (TCO3) is not provided by ERA5, but it can be computed by vertically
142   integrating the ozone mixing ratio (RO3) divided by the gravitational acceleration:

143    $\text{TCO3} = \frac{1}{g} \iint_{Ps}^{0} \text{RO3} \, dp$, where *Ps* is the surface pressure, and *g* is the gravitational

144   acceleration constant ($g = 9.8$ m/s^2) The units of the TCO3 is converted from kg/m^2 to
145   Dobson Unit (DU) with a rough estimate of 1 DU = 2.1415×10^{-5} kg/m^2
146   (http://www.temis.nl/general/dobsonunit.html; Zhang et al., 2019). ERA5 assimilates 19
147   different ozone observation sources during different periods since 1979 (Fig. 7 in Hersbach et
148   al., 2020), so it is reasonable to use TCO3 from this modern reanalysis as a reference state.

149   The monthly Niño3.4 index is used to identify the phase of the El Niño-Southern
150   Oscillation (ENSO). The sea surface temperature (SST) data are collected by the Japanese
151   Meteorological Agency (COBE SST) and sourced from PSL, NOAA
152   (https://psl.noaa.gov/data/gridded/data.cobe.html). In addition, the quasi biennial oscillation
153   (QBO) time series shared by Berlin Free University
154   (https://www.geo.fu-berlin.de/en/met/ag/strat/produkte/qbo/index.html) is also used to test the
155   potential predictability source.

156   *2.3 Methods*

157   To assess the predictability of ozone and circulation anomaly distributions, the pattern
158   correlation coefficient (PCC) between forecasts and the reanalysis for a variable *V* is utilized,

159    $\text{PCC} = \frac{\sum_{i=1}^{n} w(i)[V_{\text{FC}}(i) - \overline{V_{\text{FC}}}][V_{\text{RE}}(i) - \overline{V_{\text{RE}}}]}{\sqrt{\sum_{i=1}^{n} w(i)[V_{\text{FC}}(i) - \overline{V_{\text{FC}}}]^2} \sqrt{\sum_{i=1}^{n} w(i)[V_{\text{RE}}(i) - \overline{V_{\text{RE}}}]^2}}$. In the PCC formula, *i* is the spatial grid

160   index, *n* is the total number of spatial grid points in the extratropics (30–90°N). The subscript
161   "FC" denotes the model forecast, and "RE" denotes the ERA5 reanalysis. The overbars in the
162   PCC formula denote spatial averages.

163   The following metrics are used to track the relationship between the stratospheric polar
164   vortex and the Arctic total ozone: (1) the polar cap height area-weighted over 60–90°N at
165   50hPa; (2) polar total ozone area-weighted over 60–90°N [Strahan et al. (2013) used the 63–
166   90°N means]; (3) days of strong polar vortex during December–February (DJF) with the
167   zonal-mean zonal winds at 60°N and 10hPa greater than 35 or 40 m/s; (4) another metric for
168   the polar vortex strength, zonal-mean zonal winds at 60°N and 10hPa in DJF; (5) the volume
169   of the polar stratospheric clouds (V_{PSC}) in late winter (February–March, FM), estimated as

170   $V_{PSC} = (0.8 \times A_{PSC}@50\text{hPa} + 0.2 \times A_{PSC}@30\text{hPa}) \times 5.06\text{km}$, where $A_{\text{PSC}}@50\text{hPa}$ is the

171   area at 50 hPa colder than 195.59 K and $A_{\text{PSC}}@30\text{hPa}$ is the area at 30hPa colder than 193.61

172   K (Rex et al., 2004; Rieder & Polvani, 2013; Garfinkel et al., 2015). The third and fifth

173   indices are calculated using the ERA5 daily means, and the others are based on the monthly

174   means.

3. Backgrounds for the three historical Artic ozone holes

176   Figure 1 shows the time series of several metrics, including the Arctic total column

177   ozone versus polar cap height at 50 hPa in March (Figure 1a), days of strong polar vortex in

178   DJF (Figure 1b), the winter-mean polar jet intensity versus late winter V_{PSC} (Figure 1c), and

179   two dominant tropical forcings (ENSO and QBO). It is evident that polar cap height and

180   ozone in March 1997, 2011, and 2020 rank as the top three low values from 1979–2020

181   (Figure 1a). The high correlation (i.e., 0.80) between polar cap height and the Arctic total

182   ozone might indicate that they are strongly coupled with each other. Based on this, Seviour et

183   al. (2014) designed a statistical plus dynamical forecast procedure but for seasonal prediction

184   of the Antarctic ozone, although the GloSea5 forecast system does not include a diagnostic

185   chemical module. The formation of low Arctic ozone concentrations is also preceded by a

186   quiescent winter with a strong stratospheric polar vortex (Figures 1b, 1c), indicating a weak

187   residual circulation (not shown). A strong and cold polar vortex allows for the formation of

188   more polar stratospheric clouds (Figure 1c) and chlorine activation (Manney et al., 2011;

189   Arnone et al., 2012), whereby the depletion of ozone is larger than normal. In addition, no

190   midwinter SSW appeared before the three ozone hole events, and the final warming did not

191   happen until April (e.g., 30 April 1997, 5 April 2011, 29 April 2020). Our results do not

192   suggest any directly significant relationship between ENSO and the Arctic total ozone, but

193   the QBO indeed contributes marginally to interannual variability of March ozone (Figure 1d).

194   Hurwitz et al. (2011) also emphasize the possible impact of warm SST anomalies in North

195   Pacific on the strong polar vortex in March 2011, which were not observed in the 1996/97

196   and 2019/20 winters (not shown).

197   Figure 2 compares the meteorological conditions for the three Arctic ozone hole events.

198   The climatological ozone is around 420 DU in March (Figure 2a), but the lowest

199   column-ozone is below 280 DU for the three holes (Figures 2b–2d). The minimum ozone

200   value over the Arctic in March 2020 is even lower than in 2011 and 1997, and the position of

201   the low center is also different among the events: towards North America in March 2020,

202   symmetric about the pole in March 2011, but towards Eurasia in March 1997. Such a

203   displacement of the low-ozone center is consistent with the shape of the stratospheric polar

204   vortex at 10hPa (similar at 50hPa) denoted by the high PV value (Figures 2e–2h) and low

205   height anomalies at 50 hPa (Figure S1). On average, the polar vortex begins to weaken or

206   collapse in March (Figures 2e, S1). However, in March 1997, 2011, and 2020, the polar

207   vortex was still strong, manifested by the large PV values in the Arctic at 10 hPa (>600 PVU).

208   The PV maximum was located in Arctic Canada in March 2020, near the North Pole in

209   March 2011, and shifted towards Arctic Russia in March 1997 (Figures 2f–2h). Therefore, the

210   Arctic ozone hole is coupled with an extremely strong stratospheric polar vortex.

211   Climatologically, temperatures over the Arctic at 50hPa in March are 210–215K, well
212   above the threshold for polar stratospheric cloud formation (Figure 2i). In March 2020, 2011,
213   and 1997, the coldest temperature anomalies in the Arctic stratosphere reached ~-18K, cold
214   enough to allow for heterogeneous ozone depletion (Figures 2j–2l) that occurs more often in
215   the Antarctic and initializes radiative-dynamic feedbacks that allow the cold temperatures and
216   strong vortex to persist (Randel & Wu, 1999).

217   The residual (or Brewer-Dobson) circulation dynamically transports mass from the
218   ozone-rich tropics to the ozone-poor extratropics (Figure 2m). The strong polar vortex with
219   strong westerly jet (Figures 2i–2l) suppresses the upward propagation of waves and therefore
220   the wave-forced residual mass circulation and mixing, as is evident by the positive ozone
221   mixing ratio anomalies in tropics and negative anomalies in extratropics (Figure 2n–2p). To
222   summarize, both chemical and dynamical processes associated with a strong polar vortex
223   contributed to the formation of the Arctic ozone holes in 1997, 2011, and 2020.

4. Prediction of the Arctic ozone holes in CFSv2

225   The predictions of the March total ozone and the geopotential height (PV at pressure
226   levels is unavailable for CFSv2) anomalies from initializations at the beginning of February
227   and March are shown in Figure 3. While the early forecasts correctly forecast the sign of the
228   ozone anomalies, the anomaly amplitudes are largely underestimated (Figures 3a, 3c, 3e).
229   The early initializations better capture the 2011 ozone hole (central low: ~-80 DU) than the
230   1997 and 2020 ozone holes (central low: ~-40 DU), indicating a different predictability of
231   ozone loss for the three events. The late initializations have a similar predictive skill for the
232   three ozone holes, with a pattern correlation around 0.9 (Figures 3b, 3d, 3f). The distribution
233   of the column-ozone is largely controlled by the polar vortex both in the reanalysis (shadings)
234   and in forecasts (contours; Figures 3g–3l). The low centers of the column-ozone and height
235   anomalies are closely situated. The predictability of the column-ozone is highly consistent
236   with that of stratospheric height: the strong polar vortex in March 2011 is well forecasted in
237   the early-February initializations (Figure 3i), which exceeds the average predictive limit (~
238   two weeks) of stratospheric strong polar vortex (Domeisen et al., 2020a).

239   Rao et al. (2019, 2020b) reported that favorable external forcings such as ENSO and
240   QBO can increase the predictive limit for some SSWs. It is noticeable that the mild cold
241   ENSO state and the QBO westerly winds (Figure 1d) in the 2010/11 winter together increase
242   the possibility of a strong polar vortex in forecasts. The ENSO and QBO were nearly neutral
243   in the 1996/97 and 2019/20 winters, and the polar vortex anomalies are accurately forecasted
244   only for March initializations (Figures 3h, 3j, 3l).

245   For a forecast system without a chemical module and ozone output, the prediction of
246   ozone can be derived from a variable coupled with the ozone, e.g., the polar vortex strength.
247   An empirical prediction of the Arctic total ozone using the forecasted polar cap height (see
248   Figure S2) is shown in Figure 4. Based on the ERA5 reanalysis, the simultaneous linear
249   relationship between height and ozone is established (Figure 4a), which can then be used to
250   predict (in an empirical manner) Arctic total ozone. Figures 4c–4e assess the skill of such an

251 empirical ozone predictive model. The empirical prediction model underestimates the
252 extremity of the low-ozone in initializations earlier than March, but the empirical model can
253 well reproduce the observed anomalies in the latest initializations (March). The earlier
254 initializations (November–January) contain little skill at forecasting the ozone hole in March,
255 except that the initializations in February 2011 still have high skill possibly due to the cold
256 ENSO and westerly QBO conditions. We also assess sensitivity to basing the empirical
257 model on the regression between V_{PSC} in late winter (February–March) and the Arctic total
258 ozone (Figure 4b), and no improvement is found (not shown). Overall, the statistical model
259 might have some skill in forecasting seasonal mean polar ozone (e.g., Seviour et al., 2014),
260 but its predictive skill is too low for the March ozone hole event to reach the "hole" criterion
261 for earlier initializations.

262   The direct prediction of ozone from the chemical module in CFSv2 is similar to the
263 empirical prediction (Figure 5). For initializations at the beginning of March, nearly all of the
264 Arctic ozone anomalies can be reproduced by CFSv2 (Figures 5a–5c). For initializations in
265 early February 2011, most of the negative Arctic ozone anomalies in March 2011 are
266 forecasted (Figure 5b). The pattern correlation of the extratropical total ozone is also much
267 larger for initializations in March than other winter months (Figures 5d–5f). These results
268 suggest that March Arctic ozone hole events can be accurately predicted on March 1 or
269 earlier.

5. Conclusions

271   Since 1979, three March ozone holes have been observed with a monthly minimum of
272 Arctic total ozone lower than 280 DU: 1997, 2011, and 2020. Unlike the Antarctic ozone hole
273 that has formed every spring since the 1980s, an Arctic ozone hole has happened only every
274 one or two decades. A timely and accurate warning of the formation of ozone hole is of vital
275 importance for ecosystems in subpolar regions. Namely, reduced ozone in the stratosphere
276 lets more ultraviolet radiation reach the near surface and harm life in high latitudes after the
277 spring equinox. Based on the ERA5 reanalysis, observations, and seasonal forecasts by
278 CFSv2, the meteorological backgrounds of the historical Arctic ozone holes and their
279 predictability using an empirical model and a dynamical model are assessed.

280   Some similarities are found for the three ozone hole events: 1) No midwinter SSWs
281 happened before the March ozone hole events, which is consistent with the extremely strong
282 polar vortex throughout the winter, as well as more days in DJF with a strong westerly jet and
283 with extremely cold temperatures that allow for polar stratospheric clouds to form (denoted
284 by large V_{PSC}). 2) The final warming occurred in April for the three ozone hole events, after
285 the ozone hole already had time to develop. 3) The ozone low center is mainly controlled by
286 the simultaneous polar vortex shape: displaced towards Canada and Greenland during March
287 2020, symmetrically distributed about the North Pole during March 2011, and displaced
288 towards Arctic Russia during March 1997. 4) A dipole stratospheric ozone mixing ratio
289 anomaly pattern was found for ozone hole events, that is, the positive ozone anomaly in the
290 tropical stratosphere is contrasted with the negative ozone anomaly in the extratropical

291 stratosphere.

292 Differences are also evident: 1) The backgrounds are different for the three ozone holes,
293 with the March 2011 ozone hole happening following a moderate cold ENSO state and a
294 weak QBO westerly in winter. However, the ENSO and QBO were nearly neutral in the
295 1996/97 and 2019/20 winters. 2) The 2011 ozone hole event may have been more predictable
296 than the other two due to favorable conditions for a strong stratospheric polar vortex.The
297 CFSv2 is among the best models at predicting the stratospheric evolution (Domeisen et al.,
298 2020a, 2020b; Garfinkel et al., 2020; Rao et al., 2019, 2020a, 2020b), and hence we expect
299 that our conclusions will be representative of other state-of-the-art models with a chemistry
300 module.

301 We also find that the ozone predicted from an empirical model using model output is
302 nearly as skillful as ozone actually predicted by the model itself. This similarity implies that
303 one can use models in the S2S archive (which do not archive ozone) to study predictability of
304 ozone hole events. Namely, the intensity of the stratospheric polar vortex in March and V_{PSC}
305 calculated based on temperatures, are a good substitute index for Arctic ozone prediction. We
306 leave for future work a more detailed study of empirical prediction of ozone based on
307 forecasted polar vortex metrics in other S2S models.

Acknowledgements

References

321 Arnone, E., Castelli, E., Papandrea, E., Carlotti, M., & Dinelli, B. M. (2012). Extreme ozone
322 depletion in the 2010-2011 Arctic winter stratosphere as observed by MIPAS/ENVISAT
323 using a 2-D tomographic approach. *Atmospheric Chemistry and Physics, 12*(19), 9149–
324 9165. https://doi.org/10.5194/acp-12-9149-2012
325 Calvo, N., Polvani, L. M., & Solomon, S. (2015). On the surface impact of Arctic
326 stratospheric ozone extremes. *Environmental Research Letters, 10*(9), 094003.
327 https://doi.org/10.1088/1748-9326/10/9/094003
328 Chipperfield, M. P., Dhomse, S. S., Feng, W., McKenzie, R. L., Velders, G. J. M., & Pyle, J.
329 A. (2015). Quantifying the ozone and ultraviolet benefits already achieved by the

Montreal Protocol. *Nature Communications, 6,* 7233. https://doi.org/10.1038/ncomms8233

Compo, G. P, Moorthi, S. Lu, S., Long, C. S., Lee, H. T., McCormack, J. P., Sardeshmukh, P. D., & Whitaker, J. S. (2016). Improving the prognostic ozone parameterization in the NCEP GFS and CFS for climate reanalysis and operational forecasts. Paper presented at *28th Conference on Climate Variability and Change* (a session of *96th American Meteorological Society Annual Meeting*), American Meteorological Society, New Orleans, Louisiana.

Domeisen, D. I. V., Butler, A. H., Charlton-Perez, A. J., Ayarzagüena, B., Baldwin, M. P., Dunn-Sigouin, E., . . . Taguchi, M. (2020a). The Role of the stratosphere in subseasonal to seasonal prediction: 1. Predictability of the stratosphere. *Journal of Geophysical Research: Atmospheres, 125*(2), e2019jd030920. https://doi.org/10.1029/2019jd030920

Domeisen, D. I. V., Butler, A. H., Charlton-Perez, A. J., Ayarzagüena, B., Baldwin, M. P., Dunn-Sigouin, E., . . . Taguchi, M. (2020b). The role of the stratosphere in subseasonal to seasonal Prediction: 2. Predictability arising from stratosphere-troposphere coupling. *Journal of Geophysical Research: Atmospheres, 125*(2), e2019jd030923. https://doi.org/10.1029/2019jd030923

Garfinkel, C. I., Hurwitz, M. M., & Oman, L. D. (2015). Effect of recent sea surface temperature trends on the Arctic stratospheric vortex. *Journal of Geophysical Research: Atmospheres, 120*(11), 5404–5416. https://doi.org/10.1002/2015jd023284

Garfinkel, C. I., Schwartz, C., White, I. P., & Rao, J. (2020). Predictability of the early winter Arctic Oscillation from Autumn Eurasian snowcover in subseasonal forecast models. *Climate Dynamics*, in press.

Harari, O., Garfinkel, C. I., Ziskin Ziv, S., Morgenstern, O., Zeng, G., Tilmes, S., . . . Davis, S. (2019). Influence of Arctic stratospheric ozone on surface climate in CCMI models. *Atmospheric Chemistry and Physics, 19*(14), 9253–9268. https://doi.org/10.5194/acp-19-9253-2019

Harris, N. R. P., Lehmann, R., Rex, M., & von der Gathen, P. (2010). A closer look at Arctic ozone loss and polar stratospheric clouds. *Atmospheric Chemistry and Physics, 10*(17), 8499–8510. https://doi.org/10.5194/acp-10-8499-2010

Hersbach, H., Bell, B., Berrisford, P., Hirahara, S., Horányi, A., Muñoz-Sabater, J., . . . Thépaut, J. N. (2020). The ERA5 Global Reanalysis. *Quarterly Journal of the Royal Meteorological Society*. https://doi.org/10.1002/qj.3803

Hommel, R., Eichmann, K. U., Aschmann, J., Bramstedt, K., Weber, M., von Savigny, C., . . . Burrows, J. P. (2014). Chemical ozone loss and ozone mini-hole event during the Arctic winter 2010/2011 as observed by SCIAMACHY and GOME-2. *Atmospheric Chemistry and Physics, 14*(7), 3247–3276. https://doi.org/10.5194/acp-14-3247-2014

Hurwitz, M. M., Newman, P. A., & Garfinkel, C. I. (2011). The Arctic vortex in March 2011: a dynamical perspective. *Atmospheric Chemistry and Physics, 11*(22), 11447–11453. https://doi.org/10.5194/acp-11-11447-2011

Ivy, D. J., Solomon, S., Calvo, N., & Thompson, D. W. J. (2017). Observed connections of Arctic stratospheric ozone extremes to Northern Hemisphere surface climate.

Environmental Research Letters, 12(2), 024004.
https://doi.org/10.1088/1748-9326/aa57a4

Liu, N. Q., Huang, F. X., & Wang, W. H. (2011). Monitoring of the 2011 spring low ozone events in the Arctic region. *Chinese Science Bulletin, 56*(27), 2893–2896. https://doi.org/10.1007/s11434-011-4636-3

Manney, G. L., Santee, M. L., Rex, M., Livesey, N. J., Pitts, M. C., Veefkind, P., . . . Zinoviev, N. S. (2011). Unprecedented Arctic ozone loss in 2011. *Nature, 478*(7370), 469–475. https://doi.org/10.1038/nature10556

McCormack, J. P., Eckermann, S. D., Siskind, D. E., & McGee, T. J. (2006). CHEM2D-OPP: A new linearized gas-phase ozone photochemistry parameterization for high-altitude NWP and climate models. *Atmospheric Chemistry and Physics, 6*(12), 4943–4972. https://doi.org/10.5194/acp-6-4943-2006

Neely, R. R., Marsh, D. R., Smith, K. L., Davis, S. M., & Polvani, L. M. (2014). Biases in southern hemisphere climate trends induced by coarsely specifying the temporal resolution of stratospheric ozone. *Geophysical Research Letters, 41*(23), 8602–8610. https://doi.org/10.1002/2014gl061627

Newman, P. A., Gleason, J. F., McPeters, R. D., & Stolarski, R. S. (1997). Anomalously low ozone over the Arctic. *Geophysical Research Letters, 24*(22), 2689–2692. https://doi.org/10.1029/97gl52831

Olascoaga, M. J., Brown, M. G., Beron-Vera, F. J., & Koçak, H. (2012). Brief communication "Stratospheric winds, transport barriers and the 2011 Arctic ozone hole&quot. *Nonlinear Processes in Geophysics, 19*(6), 687–692. https://doi.org/10.5194/npg-19-687-2012

Previdi, M., & Polvani, L. M. (2014). Climate system response to stratospheric ozone depletion and recovery. *Quarterly Journal of the Royal Meteorological Society, 140*(685), 2401–2419. https://doi.org/10.1002/qj.2330

Randel, W. J., & Wu, F. (1999). A stratospheric ozone trends data set for global modeling studies. *Geophys. Res. Lett., 26*(20), 3089–3092. https://doi.org/10.1029/1999gl900615

Rao, J., Garfinkel, C. I., Chen, H., & White, I. P. (2019). The 2019 New Year stratospheric sudden warming and its real-time predictions in multiple S2S models. *Journal of Geophysical Research: Atmospheres*, 124(21), 11155–11174. https://doi.org/10.1029/2019JD030826

Rao, J., Garfinkel, C. I., & White, I. P. (2020). Predicting the downward and surface influence of the February 2018 and January 2019 sudden stratospheric warming events in Subseasonal to Seasonal (S2S) models. *Journal of Geophysical Research: Atmospheres*, 125(2), e2019JD031919. https://doi.org/10.1029/2019JD031919

Rao, J., Garfinkel, C. I., White, I. P., & Schwartz, C. (2020b). The Southern Hemisphere sudden stratospheric warming in September 2019 and its predictions in S2S models. *Journal of Geophysical Research: Atmospheres*.

Rex, M., Salawitch, R. J., von der Gathen, P., Harris, N. R. P., Chipperfield, M. P., & Naujokat, B. (2004). Arctic ozone loss and climate change. *Geophysical Research Letters, 31*(4), L04116. https://doi.org/10.1029/2003gl018844
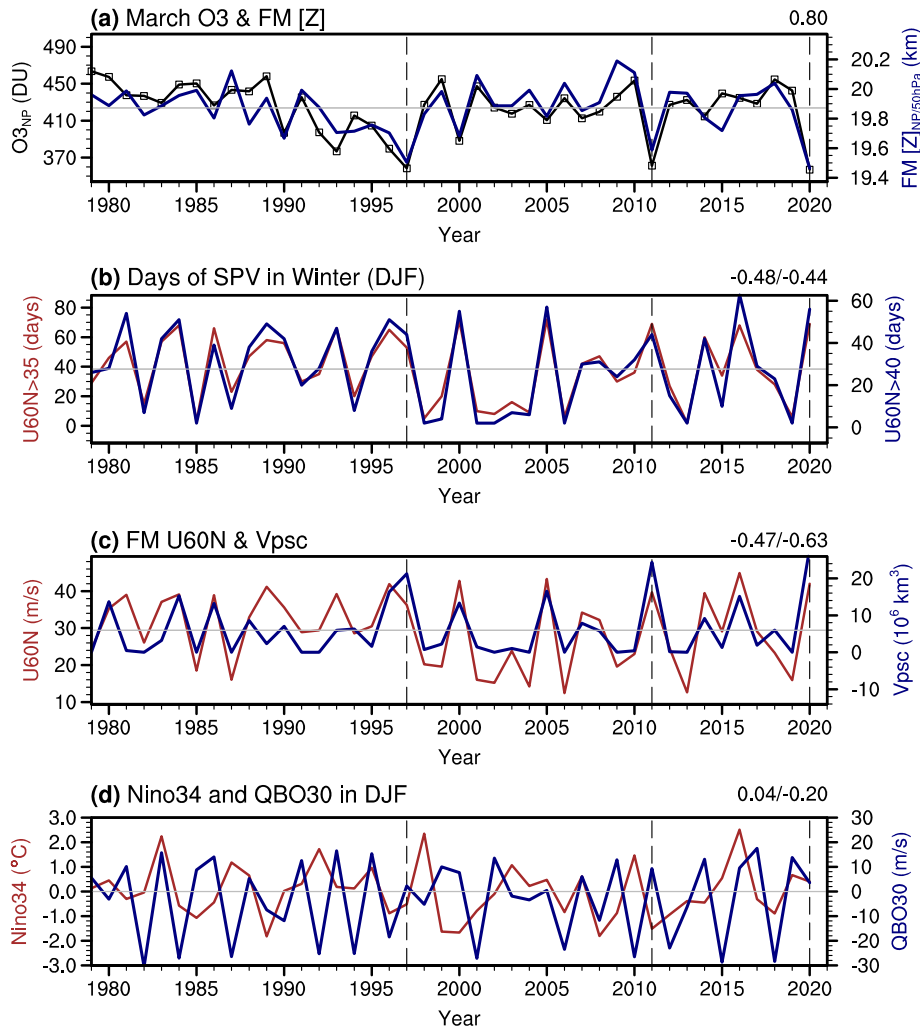
414 Rex, M., Salawitch, R. J., Deckelmann, H., von der Gathen, P., Harris, N. R. P., Chipperfield,
415   M. P., . . . Zerefos, C. (2006). Arctic winter 2005: Implications for stratospheric ozone
416   loss and climate change. *Geophysical Research Letters, 33*(23), L23808.
417   https://doi.org/10.1029/2006gl026731

418 Rieder, H. E., & Polvani, L. M. (2013). Are recent Arctic ozone losses caused by increasing
419   greenhouse gases? *Geophysical Research Letters, 40*(16), 4437–4441.
420   https://doi.org/10.1002/grl.50835

421 Rieder, H. E., Polvani, L. M., & Solomon, S. (2014). Distinguishing the impacts of
422   ozone-depleting substances and well-mixed greenhouse gases on Arctic stratospheric
423   ozone and temperature trends. *Geophysical Research Letters, 41*(7), 2652–2660.
424   https://doi.org/10.1002/2014gl059367

425 Saha, S., Moorthi, S., Wu, X., Wang, J., Nadiga, S., Tripp, P., . . . Becker, E. (2014). The
426   NCEP climate forecast system version 2. *Journal of Climate, 27*(6), 2185–2208.
427   https://doi.org/10.1175/jcli-d-12-00823.1

428 Seviour, W. J. M., Hardiman, S. C., Gray, L. J., Butchart, N., MacLachlan, C., & Scaife, A. A.
429   (2014). Skillful seasonal prediction of the Southern Annular mode and Antarctic ozone.
430   *Journal of Climate, 27*(19), 7462–7474. https://doi.org/10.1175/jcli-d-14-00264.1

431 Shaw, T. A., & Perlwitz, J. (2014). On the control of the residual circulation and stratospheric
432   temperatures in the Arctic by planetary wave coupling. *Journal of the Atmospheric
433   Sciences, 71*(1), 195–206. https://doi.org/10.1175/jas-d-13-0138.1

434 Sinnhuber, B. M., Stiller, G., Ruhnke, R., von Clarmann, T., Kellmann, S., & Aschmann, J.
435   (2011). Arctic winter 2010/2011 at the brink of an ozone hole. *Geophysical Research
436   Letters, 38*(24), L24814. https://doi.org/10.1029/2011gl049784

437 Solomon, S., Haskins, J., Ivy, D. J., & Min, F. (2014). Fundamental differences between
438   Arctic and Antarctic ozone depletion. *Proceedings of the National Academy of Sciences
439   of the United States of America, 111*(17), 6220–6225.
440   https://doi.org/10.1073/pnas.1319307111

441 Solomon, S. (1999). Stratospheric ozone depletion: A review of concepts and history.
442   *Reviews of Geophysics, 37*(3), 275–316. https://doi.org/10.1029/1999rg900008

443 Strahan, S. E., Douglass, A. R., & Newman, P. A. (2013). The contributions of chemistry and
444   transport to low arctic ozone in March 2011 derived from Aura MLS observations.
445   *Journal of Geophysical Research: Atmospheres, 118*(3), 1563–1576.
446   https://doi.org/10.1002/jgrd.50181

447 Thompson, D. W., & Solomon, S. (2002). Interpretation of recent Southern Hemisphere
448   climate change. *Science, 296*(5569), 895–899. https://doi.org/10.1126/science.1069270

449 Varotsos, C. A., Cracknell, A. P., & Tzanis, C. (2012). The exceptional ozone depletion over
450   the Arctic in January-March 2011. *Remote Sensing Letters, 3*(4), 343–352.
451   https://doi.org/10.1080/01431161.2011.597792

452 Waugh, D. W., Oman, L., Newman, P. A., Stolarski, R. S., Pawson, S., Nielsen, J. E., &
453   Perlwitz, J. (2009). Effect of zonal asymmetries in stratospheric ozone on simulated
454   Southern Hemisphere climate trends. *Geophysical Research Letters, 36*(18), L18701.
455   https://doi.org/10.1029/2009gl040419

456   Zhang, Y., Wang, W., Li, X., Zhang, X., Zheng, Z., & Liu, R. (2013). Anomalously low
457   ozone of 1997 and 2011 Arctic spring: Monitoring results and analysis. *Advances in*
458   *Polar Science, 23*(2), 82–86. https://doi.org/10.3724/sp.J.1085.2012.00082
459   Zhang, Z. Rao, J., Guo, D., Zhang, W., Li, L., Tang, Z., Shi, C., Su, Y., & Zhang, F. (2019).
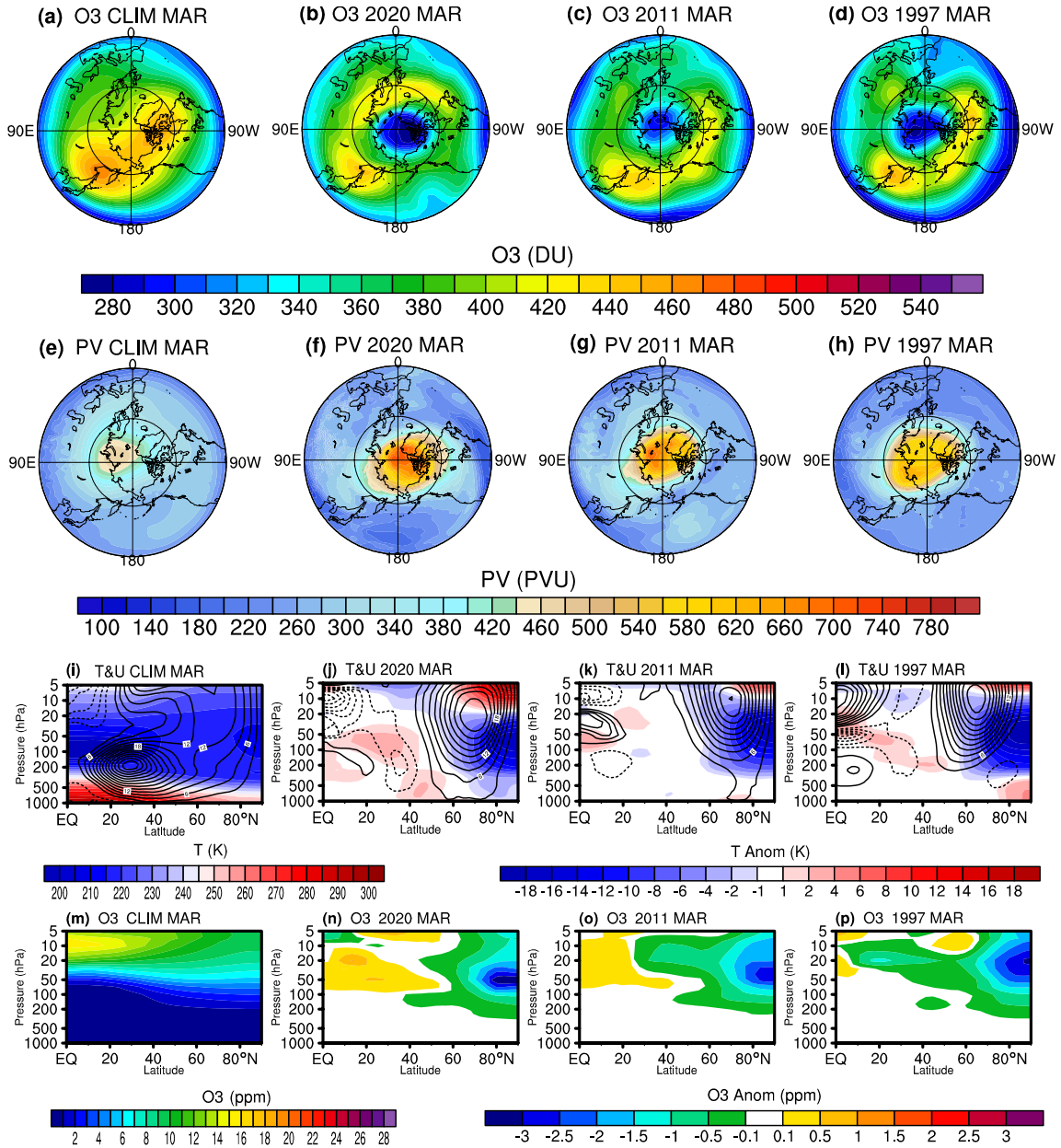460   Interdecadal variations of the midlatitude ozone valleys in summer. *Atmosphere*, 10(11),
461   677. https://doi/org/10.3390/atmos10110677
462
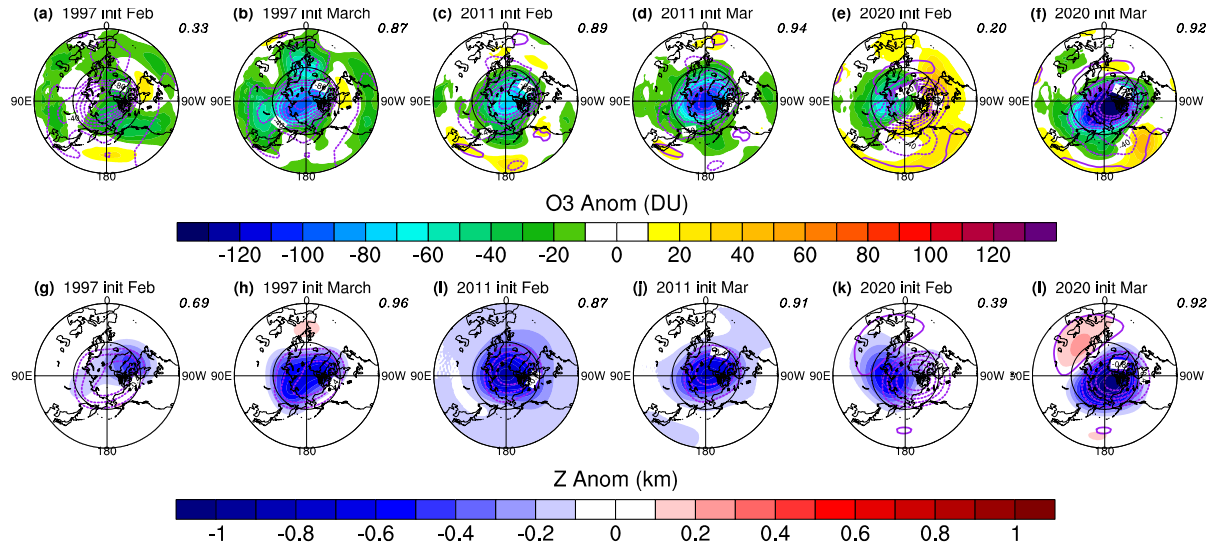
463 **Figures and captions**

464

465 **Figure 1.** (a) Time series of the polar (60–90°N) ozone (units: DU, left ordinate) in March
466 and 50-hPa height (units: km, right column) in late winter (February–March, FM hereafter)
467 from 1979–2020 in the ERA5 reanalysis. (b) Days of strong polar vortex in December–
468 February (DJF) with the zonal mean zonal wind at 10hPa and 60°N greater than 35 m/s (left
469 ordinate) and 40 m/s (right ordinate), respectively. (c) Time series of the zonal mean zonal
470 wind in FM at 10hPa and 60°N and the volume of polar stratospheric clouds (V_{PSC}) in FM. (d)
471 The time series of the winter-mean Niño3.4 index (units: °C, left ordinate) and the QBO
472 index (units: m/s, right ordinate) at 30 hPa (QBO30). The correlation between each index and
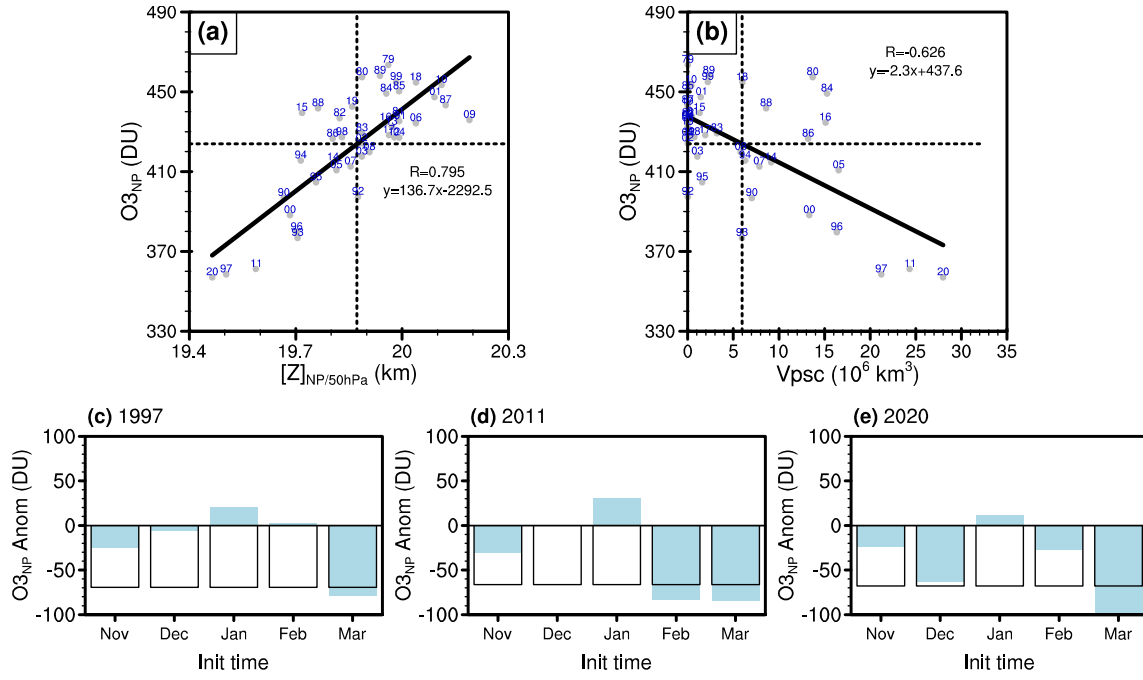473 the March ozone is also printed on the top right in each plot.

474

Figure 2. (a–d) The climatological distribution of March ozone (units: DU) in the extratropics and three historical March ozone hole events in 1997, 2011, and 2020, respectively. (e–f) As in (a–d) but for the distribution of the March potential vorticity (PV). (i) Latitude-pressure cross section of the climatological zonal-mean temperature (shadings, units: K) and zonal-mean zonal wind (contours, units: m/s) in March. (j–l) As in (i) but for the temperature and zonal wind anomalies in March 1997, 2011, and 2020, respectively. (m–p) As in (i–l) but for the latitude-pressure cross section of the ozone concentration (units: ppm). Note that the climatology (i, m) and anomalies (j–l, n–p) in the last two rows use different color scales.
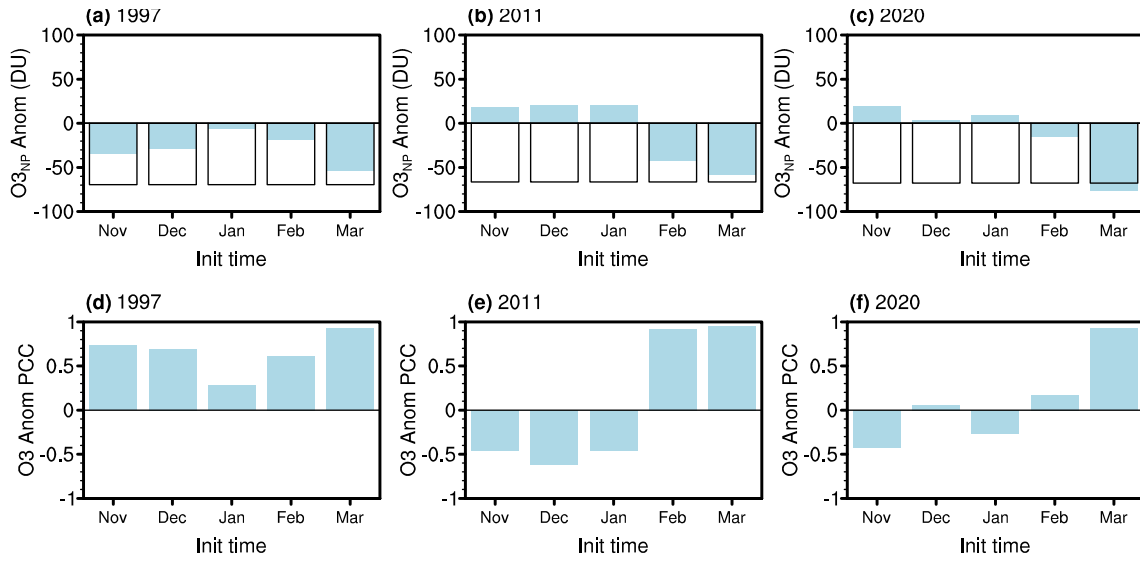
Figure 3. (a). CFSv2 predictions of the total ozone anomalies (first row, units: DU) and height anomalies at 50 hPa (second row, units: km) in shadings. The contours show the observed anomalies from the ERA5 reanalysis, with an ozone interval of 20 DU and height interval of 0.2 km (zero skipped). The first two columns (a, b, g, h) show predictions for the 1997 March ozone hole, the middle two columns (c, d, i, j) show predictions for the 2011 March ozone hole, and the last two columns (e, f, k, l) show prediction for the 2020 March ozone hole. Only predictions initialized at the beginning of February (a, c, e, g, i, k) and March (b, d, f, h, j, l) are shown.

Figure 4. (a) Scatterplot of the polar cap height at 50hPa in FM (units: km) versus the polar cap total ozone in March (units: DU). The year is marked with a two-digital integer. The horizontal and vertical dashed lines are the mean of the March polar cap height at 10 hPa and total ozone, respectively. The thick line is the linear regression between the height and total ozone. (b) As in (a) but for scatterplot of the volume of polar stratospheric clouds in FM (V_{PSC}; units: $10^6 km^3$) versus the total ozone area-averaged over the polar cap region in March. (c–e) Empirical predictions of the polar cap total ozone in March (units: DU) using the forecasted polar cap height anomalies (i.e., $137.6 \times$ height anomalies). The empirical predictions of the polar cap total ozone in March using the forecasted V_{PSC} anomalies are similar (not shown).

508

509 **Figure 5.** (a–c) CFSv2 predictions of the total ozone anomalies (units: DU) in March over the
510 polar cap (60–90°N) for the three historical ozone hole events in 1997, 2011, and 2020. The
511 abscissa shows the initialization time at the beginning of each month, and four members are
512 available. The filled histogram shows the forecast, and the unfilled histogram shows the
513 ERA5 reanalysis. (d–f) As in (a–c) but for pattern correlations between the forecasts and the
514 reanalysis.